# The mutational steps of SARS-CoV-2 to become like Omicron within seven months: the story of immune escape in an immunocompromised patient

Sissy Therese Sonnleitner[1,2]*, Martina Prelog[3]*, Stefanie Sonnleitner[1], Eva Hinterbichler[1], Hannah Halbfurter[1], Dominik B. C. Kopecky[1], Giovanni Almanzar[3], Stephan Koblmüller[4], Christian Sturmbauer[4], Leonard Feist[5], Ralf Horres[5],Wilfried Posch[2], Gernot Walder[1].

[1] Dr. Gernot Walder GmbH, Medical Laboratory, Department of Virology, 9931 Ausservillgraten 30, Austria.

[2] Institute of Hygiene and Medical Microbiology, Medical University of Innsbruck, 6020 Innsbruck, Austria.

[3] Pediatric Rheumatology/Special Immunology, Department of Pediatrics, University Hospital Wuerzburg, Josef-Schneider-Str. 2, Wuerzburg, Germany.

[4] Institute of Biology, University of Graz, Universitätsplatz 2, 8010 Graz, Austria.

[5] GenXPro GmbH, Altenhoeferallee 3, 60438 Frankfurt am Main, Germany

*These authors contributed equally.

Corresponding author: sissy.sonnleitner@infektiologie.tirol

## ABSTRACT

We studied a unique case of prolonged viral shedding in an immunocompromised patient that generated a series of SARS-CoV-2 immune escape mutations over a period of seven months. During the persisting SARS-CoV-2 infection seventeen non-synonymous mutations were observed, thirteen (13/17; 76.5%) of which occurred in the genomic region coding for spike. Fifteen (15/17; 88.2%) of these mutations have already been described in the context of variants of concern and include the prominent immune escape mutations S:E484K, S:D950N, S:P681H, S:N501Y, S:del(9), N:S235F and S:H655Y. Fifty percent of all mutations acquired by the investigated strain (11/22) are found in similar form in the Omicron variant of concern. The study shows the chronology of the evolution of intra-host mutations, which can be seen as the straight mutational response of the virus to specific antibodies and should therefore be given special attention in the rating of immune escape mutations of SARS-CoV-2.

## INTRODUCTION

In December 2019 the Wuhan Municipial Health Commission (China) reported a cluster of cases of pneumonia of unknown etiology to the WHO China Country Office. By the beginning of 2020 it was confirmed that a novel coronavirus later named severe acute respiratory syndrome coronavirus (SARS-CoV-2), was the causative agent (1). SARS-CoV-2 spreads easily and effectively among human beings with a basic reproduction number (R0) of > 2 (2, 3). Following this rapid human-to-human transmission and intercontinental spread the WHO declared a global pandemic in March of 2020. The first cases in Austria were reported in Ischgl, Tyrol, as early as February 2020 – and East Tyrol was considered one of the first hotspot areas in Central Europe.

While mutations are common in RNA viruses and mostly will not make a significant difference, some mutations proved to provide SARS-CoV-2 with a selective advantage, such as increased transmissibility or increased escape from specific antibodies (4-8). Those

variants with proven or suspected immune escape mutations were deemed variants of concern (VOC) or variants of interest (VOI), respectively, and require close monitoring (https://www.who.int/en/activities/tracking-SARS-CoV-2-variants/). The spread of the first described variant of concern (Alpha variant, B.1.1.7, VOC) was confirmed early in Austria and increased from 0.7% in January to > 99% in April 2021 in the study area East Tyrol (https://www.ages.at/themen/krankheitserreger/coronavirus/sars-cov-2-varianten-in-oesterreich/). As of December 2020, the European Center for Disease prevention and control (ECDC) noticed a sharp decline of the Alpha variant in the European Union (EU; 14.5%) followed by a fast spread of the Delta (B.1.617.2) in spring, 2021, plus a few shares of the Gamma (P1 or B.1.1.28.1, 0.3%) and others virus variants (0.3%). By January 2022, these variants have been largely replaced by the Omicron variant (B.1.1.529) in the study area. The Omicron variant now accounts for > 95% of cases. Common in these successful variants are a few specific genomic changes that give them a decisive benefit in terms of transmission or replication, e.g. in the pharynx. The most prominent spike substitutions with immune escape effect can be found in several VOC or VOI. For example, N501Y in the Alpha, Beta and Omicron variant, a nucleotide exchange at position E484 to K in the Alpha- (in a subvariant), Beta and Gamma, to Q in a Delta subvariant or to A in both Omicron subvariants BA.1 and BA.2. Furthermore, P681H is found in the Alpha and Omicron variant as well as in the VOI B.1.1.238 and the spike deletions 144/145 described as recurrent deletion regions, since they multiply occurred (9, 10).

The origin of immune escape variants is still a matter of speculation. Several hypotheses take zoonotic origin, selective pressure during treatment with antiviral drugs, monoclonal antibodies or convalescent plasma into consideration and a few studies point to the significance of the exceptional intra-host environment of immunocompromised patients to explain the evolution of immune escape variants (11-13). Those cases showed especially long-lasting viable viral shedding of SARS-CoV-2 in immunosuppressed patients for a period of more than four months (11-13). Two of the patients treated with monoclonal and convalescent plasma showed unusually high numbers of nucleotide changes and deletion mutations (12, 13), among others the already described immune escape mutation S:del69/70 (13).

In November 2020 we became aware of a patient in her 60ies with lymphoma who showed persistingly high pharyngeal viral loads of SARS-CoV-2. Although the patient had detectable SARS-CoV-2 specific antibody responses, she was unable to clear the virus load. Therefore, close monitoring was performed by rtPCR of naso-pharyngeal swabs. This unusual case prompted us to perform a thorough sequential serological screening as well as investigation of virus mutant development. Viral titre and mutant development of SARS-CoV-2 was monitored by regular naso-pharyngeal swabs with subsequent rtPCR and Next-Generation Sequencing (NGS), which enabled us to monitor the chronology of the evolution of immune escape mutations. We discuss these findings in the light of potential new sources of intra-host escape mutations and with respect to adaptations of the vaccination strategy.

## METHODSRESULTS

### Clinical presentation of an immunocompromised individual persistently infected with SARS-CoV-2

In August 2015, the patient was diagnosed with stage IVa small cell lymphocytic lymphoma, complicated by a temporary reactivation of Epstein-Barr virus (EBV) with reactive splenomegaly and rapid nodal progression. From June 2016, she was given six cycles of Rituximab and Bendamustine, which led to remission. In October 2019, the patient suffered a relapse with washout and 90% bone marrow infiltration (B-CLL Binet B or RAI III), accompanied by pronounced B symptoms and antibody deficiency. Beginning in May 2020, another round of therapy with Rituximab and Bendamustine was administered. It was completed in November 2020 after six cycles. The leukocytes counted 4200/µL in the lower normal range, platelets 136,000/µL, the immunoglobulins were clearly reduced (IgG 249 mg/dL, IgA 3 mg/dL, IgM 12 mg/dL).

Four days after the last chemotherapy – mid November 2020 - the patient fell ill with fever, cough, headache and pain, but neither loss of taste nor smell. SARS-CoV-2 was detected in the throat swab by rtPCR. The patient was in quarantine for ten days; a final PCR control was not carried out. Due to persistent fatigue, recurrent fever episodes and persistent cough with little white expectorate, the patient was again admitted to the hospital in the middle of January, 2021 and rtPCR was again positive for SARS-CoV-2. At the same time there was a recurrence of EBV. The patient was enrolled for an inhalation therapy with N-chlorotaurine (3 times daily inhalation of 10ml of N-chlorotaurine for three minutes and 10 - 14 days) (Nagl et al., 2018; Cegolon et al., 2020) and received 15g intravenous immunoglobuline (IVIG, Intratect®, Biotest Pharma GmbH, Dreieich, Germany) on admission. Ten days later; no specific therapy with antibodies against SARS-CoV-2 having been carried out - the blood findings were unchanged (leukocytes 5500/µL, platelets 102,000/µL (decreased), IgG 301 mg/dL, IgA 3 mg/dL, IgM 25 mg/dL), but the leukocyte typing showed a decline by the B-CLL of 70% and a reduction of CD4+ helper T cells. The chest x-ray was normal. The patient suffered from impaired general condition, headache and sore throat and was not able to clear SARS-CoV-2 infection. The patient again received the IVIg therapy (IVIG, Intratect®, Biotest Pharma GmbH, Dreieich, Germany). No antiviral therapeutics were administered to the patient at any time of the infection. An increase of leukocytes was developed (21,600/µL).

Since the onset of the symptoms and the first rtPCR positive swab the patient was committed to home quarantine in accordance with Austrian law. When symptoms did not clear after a month, home quarantine was slightly lightened, yet, testing with naso-pharyngeal swabs and subsequent rtPCR was continued. Persistent viral shedding was determined on day 102, day 124, day 182 and day 205 since onset of symptoms and first positive rtPCR and the viral shedding from the upper respiratory tract has continued to date (**Figure 1**). The patient gave full written consent for the case to be attended and published.

### Isolation

Isolation trials were performed from swab samples taken on day 73, 93, 99, 104, 109, 117, 127, 133 and 182 on VeroB4-cells and were successful on day 73, 93, 109 and 127. The isolation success correlated negatively with the Ct-values of the swab (k = -0.59).

**Figure 1:** Timeline of the course of disease in an immunocompromised female patient with almost continuous viral shedding throughout the study period of 207 days. Ct …Cycle

threshold; IVIG therapy … intravenous immunoglobuline therapy; RTX … Rituximab and Bendamustine therapy.

## Serology

At the same time points, specific antibodies were investigated using three different serological tools. An overview of the serological results is given in **Table 1**. On day 102 the IgG titres in general and neutralizing antibody titres in particular, were observed in a low degree with an IgG titre of 17.7 AU/mL in CLIA and a borderline titre of neutralizing antibodies of 1:4 in enzyme linked neutralisation assay (ELNA)

Humoral immune responses increased in the course of disease and yielded high values of 1320, > 2080 and 1750 AU/mL in chemiluminescent immunoassay (CLIA) and >1:32 in ELNA, on the days 124, 182 and 205, respectively. Although antibodies increased to positive activities at day 124 and were maintained, IgG avidity did not mature over time, as the RAI showed no significant increase and stayed in the low range <20%.

The analysis via immunoblot disclosed Spike 1 (S1) and the dedicated receptor-binding-domain (RBD) as the main epitopes of the IgG antibodies in the patient´s sera, whereas no IgG antibodies could be detected against the region Spike 2 (S2) or the nucleocapsid. No specific IgA antibodies were detected.

**Table 1:** Evaluation of antibody responses at different time points.

| day | CLIA (AU/mL) | ELNA (titre) | Blot IgG (AU/mL) | Activity (U/mL) | RAI (%) |
|---|---|---|---|---|---|
| **102** | positive (17.7) | borderline (1:4) | negative | 1.28 | n.d. |
| **124** | positive (1320.0) | positive (1:32) | positive S1 (209), RBD (405) | 106.7 | 2.9 |
| **182** | positive (>2080.0) | positive (>1:32) | positive S1 (294), RBD (459) | 145.5 | 17.4 |
| **250** | positive (1750.0) | positive (1:32) | positive S1 (229), RBD (353), S2 (85) | 69.1. | 22.9 |

Overview of the patient´s serological data from day 102, 124 and 182. The used diagnostic tools were the LIAISON® SARS-CoV-2 TrimericS IgG (DiaSorin S.p.A., Saluggia, Italy) (LIAISON), an Immunoblot called ViraChip® assay (Viramed, Munich, Germany), Avidity and an in-house Enzyme-Linked Neutralization Assay (ELNA) (Sonnleitner et al., 2021b). The data obtained from LIAISON® SARS-CoV-2 s1/s2 IgG CLIA assay are standardized according to the WHO criteria. CLIA … chemoluminescent immunoassay; AU/mL … arbitrary units/mL; ELNA … enzyme-linked immunosorbent assay; S1 … Spike 1; RBD … receptor-binding-domain; RAI … relative avidity index (formula: IgG concentration with chaotropic agent/IgG concentration with PBS.

## SARS-CoV-2 specific T-cell response

On day 193 no IFNg-producing SARS-CoV-2-specific immune cells could be detected in the ELISpot assay (SI = 0.86), although a significant positive reaction against pokeweed mitogen was demonstrated (mean of 213 SFU in the positive control versus mean of 1.4 SFU in the negative control and mean 1.2 SFU cells in the SARS-CoV-2-antigen stimulated wells).

## Humoral immune response did not clear SARS-CoV-2 infection

The Ct values and numbers of PFU/mL were significantly lower after day 124. The high titre of IgG antibodies of 1320 AU/mL and a neutralizing antibody titre of 1:32 analysed by our in-house assay on day 124 was associated with a significant reduction of the viral load but could not clear the infection.

We therefore decided to undertake a detailed examination of the specific genetic background of the virus population present including potential intra-host mutational dynamics.

## Mutational intra-host dynamics

Over the study period of 221 days, 14 haplotypes were sequenced out of naso-pharyngeal samples. The sequences were obtained on day 73, 93, 109, 129, 133, 136, 143, 158, 164, 171, 182, 192 and day 207 of the patient´s prolonged infection. The timeline of infection and a chronology of intra-host non-synonymous mutational events are given in **Figure 4**.

The calculation of the pairwise mutation distances did not show higher intra-host evolutionary rates in contrast to overall evolutionary rates of about (8-9) x $10^{-4}$ substitutions per year (Day et al., 2020; Dearlove et al., 2020). The pairwise distance between day 73 and day 171 was 4.4 x $10^{-4}$ in 98 days, implying a nucleotide substitution rate of 7.5 x $10^{-4}$.

All NGS sequences were shown to belong to the prevalent Pangolin lineage B.1.1. and the Nextstrain clade 20B.

We became aware of the prolonged viral shedding after about two months and started to regularly sequence the patient´s subsequent swabs as of day 73. The sequence derived from the swab of day 73 showed 18 mutations in comparison to the reference genome Wuhan (GenBank: MN908947.3, RefSeq: NC_045512.2), the sequence on day 171 had 26 substitutions which increased to 29 on day 207. A listing of all persistent and temporary non-synonymous mutations that the strain has accumulated intra-host and their concordance to variants of concern and variants of interest are given in **Table 2.** Overall, 22 non-synonymous mutations evolved over the study period of 221 days (7 months). Eleven (50%) of these non-synonymous mutations were persistent, whereas 11 (50%) occurred temporarily and were replaced by the wildtype or a different substitution. Seventeen of the 22 non-synonymous mutations evolved in the region coding for spike, eight of those were temporary. Seventeen of the 22 acquired non-synonymous mutations (77.3%) were issued as immune escape mutations by the WHO (https://www.who.int/en/activities/tracking-SARS-CoV-2-variants/) (**Figure 4**). Among the persistent non-synonymous mutations in spike, as many as 88.2% are found in various VOIs or VOCs (**Table 2**). All those genetic changes occurred after the development of high antibody titres.

One region continuously showed diffuse mutational changes, with changing temporary adaptations of substitutions and deletions, which was ORF1b: position 709 – 716.

An overview of the intra-host mutational development of SARS-CoV-2 during the study period of 221 days is given in **Table 3** and **Figure 3.**

**Table 2: Listing of all persistent and temporary non-synonymous mutations that the strain has accumulated over the 7-months study period.**

| | n total | VOC/VOI | [%] | n in spike | VOC/VOI | % |
|---|---|---|---|---|---|---|
| Acquired non-synonymous mutations: | 22 | 17 | [77.3] | 17 | 15 | [88.2] |
| Persistent non-synonymous mutations: | 11 | 8 | [72.7] | 9 | 8 | [88.9] |
| temporary non-synonymous mutations: | 11 | 9 | [81.8] | 8 | 7 | [87.5] |

n total … number of all non-synonymous intra-host acquired mutations; n in spike … number of all non-synonymous intra-host acquired mutations in the region coding for spike; VOC/VOI

…number of mutations that are found in comparable expression in a variants of concern (VOC) or a variant of interest (VOI).

**Table 3:** Overview of A) substitutions and B) deletions in the SARS-CoV-2 genome over a seven-months study period in an immunocompromised patient.

| A) | polymorphic substitutions | strain-specific sub. | acquired sub. | temporary mutations acquired and lost sub. |
|---|---|---|---|---|
| | | | **S:E484K* (day 136) β δ o** | |
| | ORF1b:D708A | E:L73F | | **ORF8:Y73C* (day 73) α** |
| | ORF1b:K709X | N:R203K | S:N354K (day 158) | **S:T716I* (day 73) α** |
| | ORF1b:Y710X | N:G204R | **S:R346I* (day 164)** | ORF3a:V255X (day 73) |
| | ORF1b:Y710L | ORF1a:L758V | ORF1a:T3284I (day 171) | S:A831V (day 117) |
| | ORF1b:V711D | ORF1a:P971S | **S:D950N* (day 171) δ γ** | **S:Y145X (day 117 - 123) o** |
| | ORF1b:V711X | ORF1a:M3221I | **S:P681H*(day 182) α** o | **S:N501Y* (day 123) α β δ o** |
| | ORF1b:R712X | ORF1a:V3976F | | **S:Y144H (day 129) o** |
| | ORF1b:V711E | **ORF1b:P314L* α δ γ** | | **S:E484Q (day 129) o** |
| | ORF1b:R712X | ORF1b:S598I | | **S:del(9) 22287* (day 136) β** |
| | ORF1b:L714X | **ORF1b:P1000L* δ γ** | | **N:S235F* (day 136) α** |
| | ORF1b:I2568X | **S:D614G* α β δ γ** S:A879S | | **S:H655Y* (day 158) δ** o |

| B) | polymorphic deletions | strain-specific del. | acquired del. |
|---|---|---|---|
| | ORF1b:K709- | ORF1a:A1204- | ORF1b:L714- (day 158) |
| | ORF1b:Y710- | ORF1a:E1205- | **S:L141- (day 164) o** |
| | ORF1b:V711- | ORF1a:I1206- | **S:G142- (day 164) o** |
| | ORF1b:R712- | ORF1a:P1207- | **S:V143- (day 164) o** |
| | ORF1b:N713- | ORF1a:K1208- | **S:Y144-* (day 171) o** |
| | ORF1b:L714- | ORF1a:E1209- | |
| | ORF1b:Q715- | ORF1a:E1210- | |
| | ORF1b:H716- | | |

Column 1 shows genetic variations in ORF1b, a region with repeated changes between substitutions and deletions, i.e. polymorphic substitutions and deletions.. Column 2 shows substitutions and deletions in comparison to the reference genome Wuhan (GenBank: MN908947.3, RefSeq: NC_045512.2), strain-specific, manifested since the beginning of the infection and maintained throughout the seven-months study period. Column 3 is a chronology of all mutations acquired by SARS-CoV-2 during the intra-host evolutionary process. * … mutations of concern or mutations which are described in the context of immune escape. Column 4 shows temporary mutational events which occurred once and did not occur any more in the following sequence. sub. … substitutions; del. … deletions α … mutations are described for the Alpha variant B.1.1.7; β … Beta variant B.1.351; δ … Gamma variant B.1.1.28.1; γ … Delta variant B.1.617.2; o … Omicron variants B.1.1.529). Underlined mutation sites are also found in the Omicron variant, but with a different substitution.

**Figure 2:** Localization of the substitutions and deletions acquired by the strain EPI_ISL_2106199 of clade 20B in the course of the prolonged infection of an immunocompromised patient. All acquired and preserved genetic adaptations occurred in the regions ORF1a (n = 1), ORF1b (n = 1) and spike (n = 9).

## Chronology of acquired mutations

In the underlying clinical case the substitutions emerged in the following chronological order:

S:Y144- emerged immediately after the increase of the specific antibody titre at day 117 as a temporary mutation, followed by E484Q (day 129), which could not assert itself against E484K and was displaced at least 7 days later (day 136). Furthermore, we found the substitutions S:N354K (day 158, 164, 171 und 182), S:R346I (day 164) and ORF1a:T3284I (day 171), S:D950N (day 171) as well as the prominent S:P681H on day 182 (Fig. 2). Three of the six acquired substitutions (50%) have already been described as typical mutations acquired by diverse variants of concern.

Thirteen of the seventeen acquired substitutions (76.5%) occurred in the genomic region coding for spike, and one each in the regions coding for ORF1a:T3284, ORF3a:V255X (day 73), ORF8:Y73C* (day 73) and N:S235F* (day 136) (**Fig. 2**).

Other mutations appeared temporarily and were subsequently replaced by the wildtype variant. Five hitherto undescribed temporary mutations were observed on the days 73 (ORF3a:V255X), 117 (S:A831V), 117 - 123 (S:Y145X), day 129 (S:Y144H), as well as on day 129 (S:E484Q, S:Y144H) (Fig. 3).

Six temporary mutations have already been described previously, all of them prominent variations known in the context of variants of concern (https://covariants.org/shared-mutations; Center for Disease Control and Prevention; https://www.cdc.gov/coronavirus/2019-ncov/variants/variant-info.html): ORF8:Y73C and S:T716I evolved in the early stage of the infection and are described in the context of the Alpha variant,. S:N501Y , known from the Alpha, Beta, Gamma and Omicron variant, S:del(9) described in the Beta variant, N:S235F, known as a typical substitution of the Alpha variant and S:H655Y, described in the context of the Beta as well as the Omicron variants. All these temporarily recurring mutational events did not establish permanently but disappeared again or were dominated again by the wildtype variant. **Figure 3** shows the acquired und temporarily acquired mutations of strain EPI_ISL_2106199 in the region coding for spike and demonstrates the high concordance of the acquired adaptations with described variants of concern, above all the Alpha and the Omicron variant (15/17; 88.2%). **Figure 3** represents the adaptations in the region coding for spike. Further mutations in the genome were ORF1a:T3284I (day 171), ORF8:Y73C (day 73), ORF3a:V255X (day 73), N:S235F (day 136), ORF1b:L714- (day 158). Thirteen of the 17 mutations (76.5%) acquired in the course of the prolonged infectious phase are already described mutations in variants of concern. Ten of the 17 spike mutations occur in a similar or identical way in the Omicron variant (58.8%). The non-synonymous mutations S:del143, S:del144, S:N501Y, S:H655Y and S:P681H were developed in identical form in the Omicron variant. Further non-synonymous mutations occurred at the amino acid positions S:142, S:144, S:145, S:484 (twice) in strain EPI_ISL_2106199 as well as in the Omicron variant, which, however, led to different expressions (S:del142 instead of S:G142D, temporarily both S:Y144H versus S:144del and S:Y145X versus S:145del as well as S:E484Q and S:E484K instead of S:E484A). Overall, 76.5% of all mutations and 88.2% of the spike mutations acquired by strain EPI_ISL_21061 convergently evolved in other variants of concern, mainly in the Alpha and the Omicron variant.

**Figure 3:** The acquired and temporarily acquired mutations of strain EPI_ISL_2106199 in the course of a seven months lasting course of infection in an immunocompromised person in the region coding for spike. Overall, 17 persistent or temporary spike mutations were evolved, whereas 9 (52.9%) turned out to be temporary and were subsequently replaced by the wild-type variant. * … temporary mutations; S1 … spike 1; S2 … spike 2; hr … heptad repeat; RBD … receptor binding domain; The mutations marked in orange are also found in the Omicron variant (B.1.1.529) in similar or identical expression (10 out of 17), mutations marked in red are found in other variants of concern (3 of 17; 17.6%). Thirteen of the 17 mutations (76.5%) acquired in the course of the prolonged infectious phase are already described mutations in variants of concern.

Overall, SARS-CoV-2 developed eleven persistent mutations during the study period of 140 days as well as eleven temporary mutational events. The chronology of intra-host mutational events is displayed in **Figure 4.**

**Figure 4:** Chronology of the emergence of intra-host mutations in an immunocompromised patient with adequate humoral and lacking cellular immune response. The study period comprised 140 days of almost permanent viral shedding. High-quality next-generation sequences could be obtained at 14 time-points during the seven-month study period (starting on day 73, ending on day 207 with the last SARS-CoV-2 positive swab) and disclosed the chronological development of mutational events of SARS-CoV-2 as an answer to a unilateral immune response with strong antibody answer but lack of specific T-cells.

In the first swab sample, whole genome sequencing did not detect any spike mutations in the investigated strain compared to the reference genome. First spike variants appeared as E484K on day 133 as a heterozygotic mutation in 41.3% of the targeted reads. On day 136 the proportion of E484K increased to 76% and, after more than seven days (day 143) the new variant dominated with 100%, but decreased to 76.8% again on day 158. On day 171 the spike variant P681H was observed for the first time with a proportion of 24% and dominated within a couple of weeks reaching 100% on day 182.

Three of the six acquired substitutions (50%) are previously described substitutions of immune escape variants, namely: S:E484K, S:D950N and S:P681H.

**Figure 5:** Chronology of the appearance of convergent intra-host mutations in a strain of the clade B.1.1., as they have been proven in identical form in the variants of concern. α … mutations are described for the Alpha variant B.1.1.7; β … Beta variant B.1.351; δ … Gamma variant B.1.1.28.1; γ … Delta variant B.1.617.2; o … Omicron variant B.1.1.529. The red line graph shows the mean frequency of all mutations at a given day. The occurrence of mutations did not occur straight-line, but in a fluctuating course, with frequent replacement by the wildtype variant.

## The fluctuating occurrence of adaptive mutations

The emergence of adaptive mutations did not occur in a linear but fluctuating fashion. Frequently, new mutations arose at a certain time point to be later replaced by the wildtype variant, again. As shown in **Figure 5**, the mutation rate shows an oscillating course with

peaks around day 125, increasing until day 182. Simultaneously, the viral load decreased continuously until the patient had several consecutive negative SARS-CoV-2 qPCR tests since day 232 and is therefore considered to be cured from COVID-19.

## Intra-host evolutionary history

The intra-host evolution of the strain EPI_ISL_2106199 from day 73 and the quasi-species arising from it in the course of the intra-host evolution form a distinct clade in the consensus tree and group together. The clade is embedded in a random composition of complete Austrian strains and variants of concern found in Europe and described and uploaded to GISAID platform in the same study period from January to May 2021 (**Figure 6**). Early Austrian sequences of the Omicron variant from December 2021 were included subsequently.

**Figure 6:** Outgroup-routed consensus tree based on 40 SARS-CoV-2 whole genome sequences with 29,806 nucleotide sites. The section highlighted in red shows the monophyletic clade of variants newly formed in an immunocompromised patient, embedded in prominent variants of concern and typical Austrian strains sequenced in the same investigation period, downloaded from GISAID and completed by early Austrian sequences of the Omicron variant in December 2021. Numbers at nodes indicate bootstrap support values (only values > 50 are shown).

## DISCUSSION

In this unique case report we described the dynamics of intra-host mutational events in an immunocompromised patient during a seven-months period of prolonged viral shedding and proven infectivity. We considered the possible influence of a quantitatively strong but regarding binding capacities probably functionally ineffective humoral antibody response and a lacking cellular immune response on the site-directed mutagenesis of SARS-CoV-2.

Our sequencing approach resulted in high-confidence variant identification and robust genome-wide coverage and enabled the establishment of a chronology of immune escape mutations. In addition, previously undescribed site-directed base-exchanges, found in the regions ORF1a and b (n = 2;ORF1a:T3284I, ORF1b:L714-), ORF3a (ORF3a:V255X) and spike protein (n = 2; S:N354K, S:A831V), were described here. Four different well-established serological methods gave insights into the humoral immune response and demonstrated the inability to clear the SARS-CoV-2 infection despite positive antibody responses. This may be due to the relatively low neutralizing ability of the detected IgG which is also supported by the low avidity of the specific IgG and impaired avidity maturation over time. Administration of IVIG was not able to enhance the clearance of SARS-CoV-2. Cellular immunity was diminished in this patient and the lack of adapted T cell-mediated immune defence may have contributed to the inefficient clearance.

The substitution rate for SARS-CoV-2 was estimated as (8-9) x $10^{-4}$ nucleotides per site per year (32). This is comparable to previously reported substitution rates of SARS-CoV (8.0-23.8 * $10^{-4}$) (33) and MERS-CoV (11.2 * $10^{-4}$) (34, 35) and comparable to the reported substitution rates for Influenza A (4-5 * $10^{-3}$) and Influenza B (2 x $10^{-3}$) virus in the haemagglutinine gene (36). From this substitution rate it can be estimated that SARS-CoV-2 undergoes about one genetic change every other week (32). In comparison, the nucleotide substitution rate per site and per year for Ebola (EBOV Makona) is estimated to be ~1.2 * $10^{-}$

$^{-3}$ (37) and for HIV-1 (3.21-4.06) * $10^{-3}$ (38). Interestingly, the evolutionary rate stayed constant throughout the first months of infection but decreased slightly after the increase of specific antibodies on day 124. We did not find elevated intra-host substitution rates compared to the general rate reported for SARS-CoV-2 (32). This unaltered intra-host evolutionary rate compared to the global average evolutionary rate suggests that these mutations in an immunocompromised patient, driven by specific antibodies, do not lead to more frequent random genomic changes, but on the contrary to very specific targeted ones.

We assume that the presence of specific antibodies forced directional selection on retaining or regaining infectiousness and thereby strongly favoured directional mutations at particular sites, acting as immune escape mutations.

E484K, a substitution in the receptor binding domain (RBD) appeared early in the course of the infection and is described to impair neutralization resistance (39), potentially compromising vaccines effectiveness (4, 6, 40-47). E484K is a well-established distinction of the variants of concern (VOC) B.1.1.7 with E484K, P.1, P.2, B.1.315, B.1.525, B.1.526 as well as B.1.617.1 (Center for Disease Control and Prevention; https://www.cdc.gov/coronavirus/2019-ncov/variants/variant-info.html). At the same position E484, both subtypes of the Omicron variant have formed the alternative substitution alanine A (Center for Disease Control and Prevention; https://www.cdc.gov/coronavirus/2019-ncov/variants/variant-info.html). On day 158, the Omicron-specific mutation S:H655Y (48, 49) could also be detected as a temporary substitution. A further genomic change in the region coding for spike was identified on position S:N354K on day 158 and had never been described before. R346I was detected in the sequence of day 164. This mutation was previously described as a reaction of SARS-CoV-2 after monoclonal antibody treatment, seeming to maintain ACE2 binding activity (50) and has also developed in the VOI Mu, 21H, B.1.621 (https://covariants.org/shared-mutations; Center for Disease Control and Prevention; https://www.cdc.gov/coronavirus/2019-ncov/variants/variant-info.html).
S:D950N arose around day 171 and is as adaptive mutation assigned to the Gamma and Delta variant (Center for Disease Control and Prevention; https://www.cdc.gov/coronavirus/2019-ncov/variants/variant-info.html).
The substitution P681H was observed for the first time in the sequence of day 171, whereby the amino acid histidine (H) first appeared as a polymorphism to become the dominant and finally fixed variant in the course of the next ten days. This transformation from proline (P) to histidine is relatively well studied and implicates a modification in the neighbouring furin cleavage site at the junction of the spike protein receptor-binding (S1) and fusion (S2) domains (51).
Another major transformation of the spike protein is the deletion of the amino acids 141 to 144. The deletions Y144/145- on the edge of the spike tip are modifications described in the VOC B.1.1.7 as the recurrent deletion region 2 (rdr2), occurring repeatedly in SARS-CoV-2 variants (9, 10).
In our case, the deletions were extended to three more deleted positions on S:141, 142 and 143. S:143del is another analogy to the Omicron variant B.1.1.592.

Nine permanent mutations were found in the spike-coding region. More precisely, four are located in the N-terminal domain (S:L141-, S:G142-, S:V143-, S:Y144-), three in the receptor-binding domain (S:R346I, S:N354K and S:E484K), both parts of S1 and three are positioned in the region encoding for S2, namely P681H in the immediate neighbourhood of the furin cleavage site and S:D905N near heptad repeat 1 as part of the fusion core region.

Of the eleven acquired adaptive mutations, only two were found outside the spike-coding regions, namely L714- in ORF1b (day 158) and T3284I in ORF1a (day 171). ORF1a and ORF1b are coding regions for non-structural proteins (nsp) (52). ORF1a:T3284I is located in the region encoding for nsp5. Nsp5 is regarded as the main protease, cleaves viral

polyprotein and works closely with nsp12 and nsp13. Together, nsp5, 12 and 13 represent the replicase machinery (52-54). ORF1b:L714- is a deletion in the region coding for nsp13, the enzyme helicase, a main component of membrane-associated replication-transcription complexes (52, 55-57).

It is remarkable that nine of the eleven persistent mutations (81.8%) acquired in the course of the prolonged infection had previously been described in the context of immune escape and were assigned to diverse variants of concern. Our bioinformatic analyses revealed that 75% of the novel mutations in our investigated strain also occur in variants of concern, whereas the highest concordance was found between strain EPI_ISL_2106199 and the Omicron variant (50%). Furthermore, we found dynamic mutational events with fluctuations between the wildtype and the variational mutation. Nine of these temporary mutations (9 of 11; 81.8%) have also been described in the context of variants of concern (Center for Disease Control and Prevention; https://www.cdc.gov/coronavirus/2019-ncov/variants/variant-info.html). In the close proximity of the acquired deletion in ORF1b:L714-, which manifested homozygously, additional conspicuous polymorphic sequences in amino acid position ORF1b:708-716 were found. We measured frequent changes in substitutions and deletions. This certainly left us with the impression of mutational escape manoeuvres. Also, this hotspot in directional mutations encodes for nsp13, the helicase.

We thus suggest that the accumulated mutations are results of an increased selection pressure on spike, the key to entering the host cell. At the same time a second process takes place intra-host, which exerts increased pressure and enforces continual reconstructions in nsp13. The findings of these temporary mutations, which almost exclusively occurred in the spike region, also fit this pattern very well.

We managed to isolate SARS-CoV-2 from swabs at different time points, which is further evidence for the continuous viability of the virus over the study period, given the evolutionary dynamics of the different sequences. The isolation success correlated negatively with the Ct value, a fact that has already been observed in previous studies (22).

Treatment with Rituximab resulting in depletion of particularly memory and effector B cells by targeting CD20 is known to cause impaired antibody responses (58-60). As naïve B cell clones are less sensitive to Rituximab treatment due to their lower expression of CD20, a robust immune response can also be assumed for those patients. Immunosuppressive therapy as well as the lymphoma disease itself may have diminished the T cellular axis of immune defence against SARS-CoV-2, which targets infected cells, and loss of control by cytotoxic T cells may have caused the ongoing replication of SARS-CoV-2 in naso-pharyngeal epithelial cells (61, 62). Impaired T cell help may have contributed to the inefficient antibody maturation.

Meanwhile, there are more studies that shed light on the evolution of immune escape variants in immunocompromised patients and support the results of our study (12, 63-69).(12, 63-69) Nonetheless, our study not only shows the accumulation of an unusually high number of immune escape mutations in a single patient, which to a strikingly high degree evolved in parallel in various variants of concern. The chronology of mutation events during seven months of infection shows a rapid accumulation of non-synonymous mutations which in part were persistent, in part temporary or even repeatedly acquired and lost.

In summary, our case report documents the medical phenomenon of persisting SARS-CoV-2 infection in an immunocompromised patient with impaired humoral and cellular immune response. Potential interference of specific antibodies led to a significant reduction in the viral load, but at the same time generated sophisticated escape mechanisms while the cell-mediated immune defence for eradication of the infection is missing. With the aid of NGS, we witnessed the directed mutational changes of SARS-CoV-2, probably facilitated by insufficient humoral immune defence. This led to the formation of highly specific virus variants, highlighting the regions exposed to the highest intra-host selective pressure. Based

on this observation one may hypothesize that immunocompromised patients pose a particular risk to establish a source of immune escape mutants of SARS-CoV-2. Our study also underlines the importance to protect these patients from SARS-CoV-2 infection by modified vaccination strategies as well as to reinforce vaccination efforts to increase herd immunity in general. Most importantly, the study points out the convergent evolution of specific mutations in SARS-CoV-2, both in VOCs, VOIs and intra-host in the strain we studied (EPI_ISL_2106199). Those specific, convergently evolving mutations reveal those neuralgic positions in the SARS-CoV-2 genome that on the one hand represent its highest fitness advantage, but on the other hand also uncovers its highest vulnerability and should be considered as the probably most important points of attack in future vaccine and therapeutics development.

## METHODS

### Immunological diagnostics

### CLIA SARS-CoV-2 TrimericS IgG

Serological tests were performed using the LIAISON® SARS-CoV-2 TrimericS IgG (DiaSorin S.p.A., Saluggia, Italy) (LIAISON), an Immunoblot called ViraChip® assay (Viramed, Munich, Germany) and an in-house enzyme-linked neutralization assay (ELNA) (14) at day 102, 124, 182 and 205 after the first positive PCR.

The LIAISON® SARS-CoV-2 TrimericS IgG is a CLIA (Chemiluminescent Immunoassay) which detects IgG antibodies reactive with the spike protein (S1/S2 domain). The assay was performed on the LIAISON® XL Analyzer according to the manufacturer's instructions and gives the arbitrary units per ml (AU/mL) according to the WHO International Standards for the Anti-SARS-CoV-2-immunoglobulin-binding activity (NIBSC 20-136).

### Microarray immunoblots

The ViraChip® assay detects temporal antibody profiles of different immunoglobulin classes against S1, S2, and nucleocapsid (N) as well as against N of the four nonSARS human coronaviruses in a commercial, miniaturized 96 wells protein microarray. The ViraChip® assay is a useful tool to identify the epitope-specificity of IgG and IgA in serum samples. The quantitative antibody measurement was performed on a ViraChip® Scanner using ViraChip® Software.

### Neutralization test

Neutralization ability of antibodies was determined performing an in-house enzyme-linked neutralization assay (ELNA) as described elsewhere (14).

### Anti-IgG-SARS ELISA

Serum IgG antibodies against SARS-CoV-2 were determined by Serion agile SARS-CoV-2 ELISA with a sensitivity of 96.2% and a specificity of 100% according to manufacturer´s instructions (Virion/Serion, Wuerzburg, Germany). Antibody activities above 15U/mL were considered positive.

### Anti-IgG-SARS-Avidity

Relative avidity index (RAI) was determined by a modification of the Serion agile SARS-CoV-2 IgG-SARS ELISA using 1M ammonium thiocyanate ($NH_4SCN$) as a chaotropic agent as described previously (15-17). RAI values were considered as: RAI > 60% high avidity, 40% < RAI < 60% as moderate, and RAI < 40% as low avidity in reference to other viral infections (18).

### SARS-CoV-2 specific T cell response

The ELISpot assay was performed using a commercially available precoated human SARS-CoV-2-specific IFN-γ ELISPOT kit according to the manufacturer´s protocol (AutoImmun Diagnostika, GmbH, Germany; Cat.no. ELSP 5500). Peripheral blood was collected into tubes coated with lithium-heparin (Vacuette, Greiner bio-one, Austria). PBMCs were separated from plasma and whole blood by gradient density (FicoLite® -H, Linaris, Germany). After washing with phosphate-buffered saline (PBS), depleting erythrocytes (RBD-Lyse Buffer Life Technologies, 1xRBC Lysis Buffer 200ml; Invitrogen eBioscience, USA REF: 00-4333-57) and washing again with PBS, cells were counted and resuspended in x-vivo medium (X-VIVO TM-10 Serum-free hematopoietic cell medium; BEBP02-055Q, Lonza, Switzerland).

Briefly, a total of 2 x $10^5$ PBMCs were incubated in duplicate with x-vivo as a negative control, pokeweed mitogen (AutoImmun Diagnostika GmbH, Germany) as a positive control,15-20mer peptide pools for SARS-CoV-2 (AutoImmun Diagnostika GmbH, Germany) and PanCorona (AutoImmun Diagnostika GmbH, Germany) for the four nonSARS human coronaviruses 229E, HKU1, NL63 and OC43 as a control of possible cellular cross-reactive responses. After incubation at 37° C for 20 hours in a sterile and humidified atmosphere, plates were washed with washing buffer (AutoImmun Diagnostika GmbH, Germany) and stained with the kit-specific reagents according to the manufacturer´s protocol. Plates were then washed several times under running water and dried overnight. Spot forming units (SFU)/100.000 cells were counted using an automated AID ELISPOT reader system (AutoImmun Diagnostika GmbH, Germany).

The assessment criteria for the ELISpots were a minimum of 50 SFU in the positive control and a maximum of 10 SFU in the negative control according to the manufacturer´s definitions (19, 20). When those criteria were fulfilled, the stimulation index (SI) was calculated by dividing the mean SFU numbers in the antigen-specific wells with the mean SFU numbers of the negative control. The test was assessed negative with an SI < 2 according to previous determination of the cut-off by well-defined pre-pandemic PBMC samples and by PBMCs from SARS-CoV-2-naive individuals. The test was suggested to be poorly reactive with an SI between 2 and 7 and reactive with an SI ≥ 7 as defined by the manufacturer (19). According to standardized laboratory procedures, in each assay, a standard laboratory control sample of a high-reactive and a non-reactive PBMC sample, respectively, was run to determine inter-assay-variations. Only assays with less than two standard deviations of the high-reactive and the non-reactive PBMC control sample, respectively, were defined valid.

**Sample collection**

Nasopharyngeal swabs were taken in a standardized way in home quarantine in the context of primary care by a medical co-worker.

**RNA extraction**

Nucleic acids were isolated using the MagMAX™-96 Total RNA Isolation Kit (Thermo Fisher Scientific, Waltham, Massachusetts, USA; Cat. No. AM1830). Briefly, 200µl PBS were taken from patient swab sample and mixed with 265µL binding buffer, 5µl proteinase K (20mg/mL) and 5µL extraction control (Thermo Fisher Scientific, Waltham, Massachusetts, USA; Cat. No. AM1830) according to the KingFisher™ extraction protocol for 200µL sample volume (Thermo Fisher Scientific, Waltham, Massachusetts, USA). After incubation at room temperature for at least 15 minutes, samples were transferred from tubes into 96-well KingFisher deep well plates (Thermo Fisher Scientific, Waltham, Massachusetts, USA) containing 280µl isopropanol and 2µL Mag-Bind particles per well, using a KingFisher™ Flex purification system (Cat. No. 5400620).

**rtPCR**

qPCR extracts were tested for SARS-CoV-2 by qRT-PCR using the Bio-Rad CFX96 system (Bio-Rad, Germany) with a LightMix Modular Assay kit in accordance with the modified

Charité guidelines (Corman et al., 2020). 10µL of extracted RNA were added into 15µL 4x Reliance One-Step Multiplex Supermix (Bio-Rad, Germany). Each 15µL mastermix contained 12.5µL buffer solution, 0.25µl enzyme mix, 1.75µL of nuclease-free water and 0.5µL primer probe wHCoV (E-Gene, as well as N-Gene and Rdrp-Gene for confirmation). Reactions were incubated at 55° C for 5 min and 95  C for 5 min in order to conduct reverse transcription of viral RNA, sample denaturation and enzyme activation. These steps were followed by PCR-amplification including 45 cycles at 95° C for 5 s, 60° C for 15 s and 72° C for 15 s. Cooling was implemented at 40° C for 30 s. Results were interpreted based on the Second Derivative Maximum (SDM) method. Positive results were confirmed by Rdrp and N-gene (21), samples with an initial Ct value lower than or equal to 37 were assigned to repeated testing including extraction. A Ct value higher than 40 was considered negative. Quantification of the viral load in the swabs was calculated via size standards of 1, 10, 100 and 1000 plaque-forming units (PFU)/mL. Standardization of viral stocks was carried out by virus titration. Isolation was performed on VeroB4 cells as described elsewhere (22).

## Virus titration

Confluent VeroB4 cells were cultured in Medium199 including 5% FCS in T75 tissue culture flasks (Sarstedt, Germany) and transferred into 96-well tissue culture plates (Sarstedt, Germany). Passage 1 isolates of SARS-CoV-2 were thawed from −80° C freezer and titrated from 1:10 to $1:10^{-12}$ in U-shaped 96-well plates (Greiner, Germany) and pipetted into each corresponding well of the 96-well tissue culture plate. Plates were incubated at 36° C. Three days post infection, incubation was stopped by gently removing the supernatant, washing the cells three times with PBS and fixing cells in 1:1 ice-cold acetone-methanol. For easier optical evaluation, cells were dyed by crystal violet staining and tissue culture infectious dose of 70% ($TCID_{70}$) and PFU were calculated (Ramakrishnan, 2016).

## Whole genome sequencing and mutational analysis

Libraries were prepared according to the Ion AmpliSeq™ SARS-CoV-2 Research Panel (Thermofisher, USA), library construction and sequencing protocol with the Library Kit Plus (Thermo Fisher Scientific, Waltham, Massachusetts, USA; Cat. No. 4488990). The Amplicons were cleaned up with AMPure XP beads (Beckman Coulter, Germany) with a 1:1 ratio. The libraries were quantified using the Ion Library TaqMan™ Quantitation Kit (Cat. No. 4468802), normalizing, pooling and sequencing was performed using an Ion Torrent™ S5 Plus. Ion Torrent Suite software (v 5.12.2) of the Ion S5 sequencer was used to map the generated reads to a SARS-CoV-2 reference genome (Wuhan-Hu-1; GenBank accession numbers NC_045512 and MN908947.3), using TMAP software included in the Torrent Suite. The following plugins were used: Coverage Analysis (v5.10.0.3), Variant Caller (v.5.12.04) for mutation calls both with “Generic  S5/S5XL (510/520/530)  Somatic  Low Stringency” and “Generic S5/S5XL (510/520/530) Germ Line Low Stringency” default parameters and COVID19AnnotateSnpEff (v.1.0.), a plugin specifically developed for SARS CoV 2 that can predict the effect of a base substitution. No ultra-deep sequencing was performed and only mutations visible in the stated analysis methods were listed and rated.

FASTA files containing the raw reads were inspected for quality criteria (mapped, targeted, filtered reads, mean depth and uniformity) using Thermofisher Software. Multiple sequence alignments were performed using Unipro UGENE (23) as well as MEGA X (Kumar et al., 2018). The SARS-CoV-2 genomes were compared to the reference NC 045512.2-Wuhan-Hu-1. Viral genome assembly and screening for distinct mutations was performed online using nextstrain.org (https://github.com/nextstrain/ncov/blob/master/defaults/clades.tsv; https://clades.nextstrain.org/). The identification of pangolin lineages was carried out using Pangolin software, v.2.4.2. (https://pangolin.cog-uk.io/). The generated full-genome sequences are available at GISAID EpiCoV (https://gisaid.org/no.EPI_ISL_2106191-21061201). Additional sequences of frequent Austrian strains and prominent variants of

623 concern, sequenced in the same study period, were retrieved from the GISAID EpiCoV
624 database (24) to calculate a consensus tree.

625 Indels were coded using 'simple indel coding' (25) as implemented in 2matrix v.1.0 (70).

626 The best-fit model of nucleotide substitutions (TIM2+F+I) was selected under the Akaike and
627 the Bayesian formation criteria using ModelFinder (71) as implemented in the PhyloSuite
628 Software package (26). Phylogenomic inference was based on a Maximum Likelihood (ML).
629 An ML tree with 5000 ultrafast bootstrap replicates was inferred in the IQ Tree plugin (27, 28)
630 of PhyloSuite.

631 **Bioinformatics CoV-Seq Workflow**

632 The frequency of the various mutations and the homology to the most widespread variants of
633 concern (Alpha-, Beta, Gamma- and Delta-variant) were investigated based on BAM files.
634 Reads from CoV-Seq samples were demultiplexed by using in-house tools. Reads
635 originating from human were filtered out by mapping against hg38 with bwa-mem 0.7.17 (29).
636 All reads not mapping to human were trimmed for adapters und quality by using Cutadapt
637 3.2(30). The trimmed reads were mapped with bwa-mem 0.7.17 to the SARS-CoV-2
638 reference MN908947.3 from the NCBI. Mutations were called using breseq 0.35.5 (31).
639 Graphics were created using *pandas* 1.2 for Python 3.

640 **Statistics**

641 Dichotomous data were evaluated by a chi-squared test or Fisher´s exacta in the case of
642 small group size ($n < 60$) (Microsoft® Excel®, Microsoft 395 MSO, Windows 10). A two-sided
643 significance level of $p < 0.05$ was used for determining statistical significance. After testing
644 for distribution (Kolmogorov-Smirnov-test), non-parametric continuous independent variables
645 were compared using Mann-Whitney-U test for each time point. Dependent non-parametric
646 variables were compared using Wilcoxon-rank test.

647

648

## ACKNOWLEDGEMENT

We gratefully acknowledge the financial support of the Austrian Research Promotion Agency (FFG), Grant No. 889135. The authors report no potential conflict of interest. We also thank Ramona Polster, MSc, for excellent technical assistance, DDI Martin Lamprecht for valuable suggestions and all the kind colleagues from the routine diagnostics team of the Dr. Gernot Walder laboratory under the direction of BSc Viktoria Muehlmann and Mag. Hannes Mahl for great support.

## AUTHOR CONTRIBUTION

**Sissy Therese Sonnleitner**: Conceptualization, Data curation, Formal analysis, Funding acquisition, Investigation, Methodology; Writing – original draft preparation. **Martina Prelog:** Writing – original draft preparation, editing; **Stefanie Sonnleitner**: Methodology, Writing – editing. **Eva Hinterbichler**: Investigation; Methodology; **Hannah Halbfurter**: Project administration. **Dominik B. C. Kopecky**: Visualization, Organization. **Giovanni Almanzar:** Methodology. **Stephan Koblmüller**: Conceptualization, Writing – editing, Funding acquisition. **Christian Sturmbauer**: Conceptualization, Writing – editing, Funding acquisition. **Leonard Feist:** Validation, Verification. **Ralf Horres:** Validation, Verification. **Wilfried Posch**: Validation, Supervision. **Gernot Walder**: Supervision.

## ETHICAL APPROVAL

All clinical samples and data were collected for routine patient care and for public health interventions. The patient gave full written consent for the case to be attended and published. Ethical approval to use residual routinely taken serum samples for retrospective analyses was obtained by the Ethics Committee of the University Hospital Wuerzburg (no. 20201105_01).

## COMPETING INTERESTS

The authors have no conflict of interest to declare.

## DATA AVAILIBILITY

The generated full-genome sequences are available at GISAID EpiCoV (https://gisaid.org/no.EPI_ISL_2106191-21061201).

## References

1. Chen L, Liu W, Zhang Q, Xu K, Ye G, Wu W, et al. RNA based mNGS approach identifies a novel human coronavirus from two individual pneumonia cases in 2019 Wuhan outbreak. Emerg Microbes Infect. 2020;9(1):313-9. Epub 20200205. doi: 10.1080/22221751.2020.1725399. PubMed PMID: 32020836; PubMed Central PMCID: PMC7033720.
2. Sanche S, Lin YT, Xu C, Romero-Severson E, Hengartner N, Ke R. High Contagiousness and Rapid Spread of Severe Acute Respiratory Syndrome Coronavirus 2. Emerg Infect Dis. 2020;26(7):1470-7. Epub 20200621. doi: 10.3201/eid2607.200282. PubMed PMID: 32255761; PubMed Central PMCID: PMC7323562.
3. D'Arienzo M, Coniglio A. Assessment of the SARS-CoV-2 basic reproduction number,. Biosaf Health. 2020;2(2):57-9. Epub 20200402. doi: 10.1016/j.bsheal.2020.03.004. PubMed PMID: 32835209; PubMed Central PMCID: PMC7148916.
4. Weisblum Y, Schmidt F, Zhang F, DaSilva J, Poston D, Lorenzi JC, et al. Escape from neutralizing antibodies by SARS-CoV-2 spike protein variants. Elife. 2020;9. Epub 20201028. doi: 10.7554/eLife.61312. PubMed PMID: 33112236; PubMed Central PMCID: PMC7723407.
5. Collier DA, De Marco A, Ferreira IATM, Meng B, Datir RP, Walls AC, et al. Sensitivity of SARS-CoV-2 B.1.1.7 to mRNA vaccine-elicited antibodies. Nature. 2021;593(7857):136-41. Epub 20210311. doi: 10.1038/s41586-021-03412-7. PubMed PMID: 33706364.

6. Liu Z, VanBlargan LA, Bloyet LM, Rothlauf PW, Chen RE, Stumpf S, et al. Identification of SARS-CoV-2 spike mutations that attenuate monoclonal and serum antibody neutralization. Cell Host Microbe. 2021;29(3):477-88.e4. Epub 20210127. doi: 10.1016/j.chom.2021.01.014. PubMed PMID: 33535027; PubMed Central PMCID: PMC7839837.
7. Müller K, Girl P, Giebl A, von Buttlar H, Dobler G, Bugert JJ, et al. Emerging SARS-CoV-2 variant B.1.1.7 reduces neutralisation activity of antibodies against wild-type SARS-CoV-2. J Clin Virol. 2021;142:104912. Epub 20210716. doi: 10.1016/j.jcv.2021.104912. PubMed PMID: 34298379; PubMed Central PMCID: PMC8282447.
8. Wang Z, Schmidt F, Weisblum Y, Muecksch F, Barnes CO, Finkin S, et al. mRNA vaccine-elicited antibodies to SARS-CoV-2 and circulating variants. Nature. 2021;592(7855):616-22. Epub 20210210. doi: 10.1038/s41586-021-03324-6. PubMed PMID: 33567448; PubMed Central PMCID: PMC8503938.
9. Harvey WT, Carabelli AM, Jackson B, Gupta RK, Thomson EC, Harrison EM, et al. SARS-CoV-2 variants, spike mutations and immune escape. Nat Rev Microbiol. 2021;19(7):409-24. Epub 20210601. doi: 10.1038/s41579-021-00573-0. PubMed PMID: 34075212; PubMed Central PMCID: PMC8167834.
10. McCarthy KR, Rennick LJ, Nambulli S, Robinson-McCarthy LR, Bain WG, Haidar G, et al. Recurrent deletions in the SARS-CoV-2 spike glycoprotein drive antibody escape. Science. 2021;371(6534):1139-42. Epub 20210203. doi: 10.1126/science.abf6950. PubMed PMID: 33536258; PubMed Central PMCID: PMC7971772.
11. Aydillo T, Gonzalez-Reiche AS, Aslam S, van de Guchte A, Khan Z, Obla A, et al. Shedding of Viable SARS-CoV-2 after Immunosuppressive Therapy for Cancer. N Engl J Med. 2020;383(26):2586-8. Epub 20201201. doi: 10.1056/NEJMc2031670. PubMed PMID: 33259154; PubMed Central PMCID: PMC7722690.
12. Choi B, Choudhary MC, Regan J, Sparks JA, Padera RF, Qiu X, et al. Persistence and Evolution of SARS-CoV-2 in an Immunocompromised Host. N Engl J Med. 2020;383(23):2291-3. Epub 20201111. doi: 10.1056/NEJMc2031364. PubMed PMID: 33176080; PubMed Central PMCID: PMC7673303.
13. Kemp SA, Collier DA, Datir R, Ferreira I, Gayed S, Jahun A, et al. Neutralising antibodies in Spike mediated SARS-CoV-2 adaptation. medRxiv. 2020. Epub 20201229. doi: 10.1101/2020.12.05.20241927. PubMed PMID: 33398302; PubMed Central PMCID: PMC7781345.
14. Sonnleitner ST, Prelog M, Jansen B, Rodgarkia-Dara C, Gietl S, Schönegger CM, et al. Maintenance of neutralizing antibodies over ten months in convalescent SARS-CoV-2 afflicted patients. Transbound Emerg Dis. 2021. Epub 20210507. doi: 10.1111/tbed.14130. PubMed PMID: 33960696; PubMed Central PMCID: PMC8242897.
15. Almanzar G, Ottensmeier B, Liese J, Prelog M. Assessment of IgG avidity against pertussis toxin and filamentous hemagglutinin via an adapted enzyme-linked immunosorbent assay (ELISA) using ammonium thiocyanate. J Immunol Methods. 2013;387(1-2):36-42. Epub 20120927. doi: 10.1016/j.jim.2012.09.008. PubMed PMID: 23022630.
16. Prelog M, Almanzar G, Rieber N, Ottensmeier B, Zlamy M, Liese J. Differences of IgG antibody avidity after an acellular pertussis (aP) booster in adolescents after a whole cell (wcP) or aP primary vaccination. Vaccine. 2013;31(2):387-93. Epub 20121108. doi: 10.1016/j.vaccine.2012.10.105. PubMed PMID: 23142306.
17. Wratil PR, Stern M, Priller A, Willmann A, Almanzar G, Vogel E, et al. Three exposures to the spike protein of SARS-CoV-2 by either infection or vaccination elicit superior neutralizing immunity to all variants of concern. Nat Med. 2022. Epub 20220128. doi: 10.1038/s41591-022-01715-4. PubMed PMID: 35090165.
18. Kneitz RH, Schubert J, Tollmann F, Zens W, Hedman K, Weissbrich B. A new method for determination of varicella-zoster virus immunoglobulin G avidity in serum and cerebrospinal fluid. BMC Infect Dis. 2004;4:33. Epub 20040908. doi: 10.1186/1471-2334-4-33. PubMed PMID: 15355548; PubMed Central PMCID: PMC522815.
19. Pantaleo G, Harari A. Functional signatures in antiviral T-cell immunity for monitoring virus-associated diseases. Nat Rev Immunol. 2006;6(5):417-23. doi: 10.1038/nri1840. PubMed PMID: 16622477.

20. Dennehy KM, Löll E, Dhillon C, Classen JM, Warm TD, Schuierer L, et al. Comparison of the Development of SARS-Coronavirus-2-Specific Cellular Immunity, and Central Memory CD4+ T-Cell Responses Following Infection versus Vaccination. Vaccines (Basel). 2021;9(12). Epub 20211207. doi: 10.3390/vaccines9121439. PubMed PMID: 34960185; PubMed Central PMCID: PMC8707815.
21. Corman VM, Landt O, Kaiser M, Molenkamp R, Meijer A, Chu DK, et al. Detection of 2019 novel coronavirus (2019-nCoV) by real-time RT-PCR. Euro Surveill. 2020;25(3). doi: 10.2807/1560-7917.ES.2020.25.3.2000045. PubMed PMID: 31992387; PubMed Central PMCID: PMC6988269.
22. Sonnleitner ST, Dorighi J, Jansen B, Schönegger C, Gietl S, Koblmüller S, et al. An in vitro model for assessment of SARS-CoV-2 infectivity by defining the correlation between virus isolation and quantitative PCR value: isolation success of SARS-CoV-2 from oropharyngeal swabs correlates negatively with Cq value. Virol J. 2021;18(1):71. Epub 20210407. doi: 10.1186/s12985-021-01542-y. PubMed PMID: 33827618; PubMed Central PMCID: PMC8025900.
23. Okonechnikov K, Golosova O, Fursov M, team U. Unipro UGENE: a unified bioinformatics toolkit. Bioinformatics. 2012;28(8):1166-7. Epub 20120224. doi: 10.1093/bioinformatics/bts091. PubMed PMID: 22368248.
24. Shu Y, McCauley J. GISAID: Global initiative on sharing all influenza data - from vision to reality. Euro Surveill. 2017;22(13). doi: 10.2807/1560-7917.ES.2017.22.13.30494. PubMed PMID: 28382917; PubMed Central PMCID: PMC5388101.
25. Simmons MP, Ochoterena H. Gaps as characters in sequence-based phylogenetic analyses. Syst Biol. 2000;49(2):369-81. PubMed PMID: 12118412.
26. Zhang D, Gao F, Jakovlić I, Zou H, Zhang J, Li WX, et al. PhyloSuite: An integrated and scalable desktop platform for streamlined molecular sequence data management and evolutionary phylogenetics studies. Mol Ecol Resour. 2020;20(1):348-55. Epub 20191106. doi: 10.1111/1755-0998.13096. PubMed PMID: 31599058.
27. Nguyen LT, Schmidt HA, von Haeseler A, Minh BQ. IQ-TREE: a fast and effective stochastic algorithm for estimating maximum-likelihood phylogenies. Mol Biol Evol. 2015;32(1):268-74. Epub 20141103. doi: 10.1093/molbev/msu300. PubMed PMID: 25371430; PubMed Central PMCID: PMC4271533.
28. Hoang DT, Chernomor O, von Haeseler A, Minh BQ, Vinh LS. UFBoot2: Improving the Ultrafast Bootstrap Approximation. Mol Biol Evol. 2018;35(2):518-22. doi: 10.1093/molbev/msx281. PubMed PMID: 29077904; PubMed Central PMCID: PMC5850222.
29. Li H, Durbin R. Fast and accurate short read alignment with Burrows-Wheeler transform. bioinformatics. 2009.
30. Martin M. Cutadapt removes adapter sequences from high-throughput sequencing reads. EMBnet journal. 2011.
31. Deatherage DE, Barrick. JE. Identification of mutations in laboratory-evolved microbes from next-generation sequencing data using breseq. Methods Mol Biol 1151. 2014.
32. Day T, Gandon S, Lion S, Otto SP. On the evolutionary epidemiology of SARS-CoV-2. Curr Biol. 2020;30(15):R849-R57. Epub 20200611. doi: 10.1016/j.cub.2020.06.031. PubMed PMID: 32750338; PubMed Central PMCID: PMC7287426.
33. Zhao Z, Li H, Wu X, Zhong Y, Zhang K, Zhang YP, et al. Moderate mutation rate in the SARS coronavirus genome and its implications. BMC Evol Biol. 2004;4:21. Epub 20040628. doi: 10.1186/1471-2148-4-21. PubMed PMID: 15222897; PubMed Central PMCID: PMC446188.
34. Cotten M, Watson SJ, Kellam P, Al-Rabeeah AA, Makhdoom HQ, Assiri A, et al. Transmission and evolution of the Middle East respiratory syndrome coronavirus in Saudi Arabia: a descriptive genomic study. Lancet. 2013;382(9909):1993-2002. Epub 20130920. doi: 10.1016/S0140-6736(13)61887-5. PubMed PMID: 24055451; PubMed Central PMCID: PMC3898949.
35. Cotten M, Watson SJ, Zumla AI, Makhdoom HQ, Palser AL, Ong SH, et al. Spread, circulation, and evolution of the Middle East respiratory syndrome coronavirus. mBio. 2014;5(1). Epub 20140218. doi: 10.1128/mBio.01062-13. PubMed PMID: 24549846; PubMed Central PMCID: PMC3944817.

36. Bedford T, Riley S, Barr IG, Broor S, Chadha M, Cox NJ, et al. Global circulation patterns of seasonal influenza viruses vary with antigenic drift. Nature. 2015;523(7559):217-20. Epub 20150608. doi: 10.1038/nature14460. PubMed PMID: 26053121; PubMed Central PMCID: PMC4499780.
37. Holmes EC, Dudas G, Rambaut A, Andersen KG. The evolution of Ebola virus: Insights from the 2013-2016 epidemic. Nature. 2016;538(7624):193-200. doi: 10.1038/nature19790. PubMed PMID: 27734858; PubMed Central PMCID: PMC5580494.
38. Duchêne S, Ho SY, Holmes EC. Declining transition/transversion ratios through time reveal limitations to the accuracy of nucleotide substitution models. BMC Evol Biol. 2015;15:36. Epub 20150311. doi: 10.1186/s12862-015-0312-6. PubMed PMID: 25886870; PubMed Central PMCID: PMC4358783.
39. Greaney AJ, Loes AN, Crawford KHD, Starr TN, Malone KD, Chu HY, et al. Comprehensive mapping of mutations in the SARS-CoV-2 receptor-binding domain that affect recognition by polyclonal human plasma antibodies. Cell Host Microbe. 2021;29(3):463-76.e6. Epub 20210208. doi: 10.1016/j.chom.2021.02.003. PubMed PMID: 33592168; PubMed Central PMCID: PMC7869748.
40. Baum A, Fulton BO, Wloga E, Copin R, Pascal KE, Russo V, et al. Antibody cocktail to SARS-CoV-2 spike protein prevents rapid mutational escape seen with individual antibodies. Science. 2020;369(6506):1014-8. Epub 20200615. doi: 10.1126/science.abd0831. PubMed PMID: 32540904; PubMed Central PMCID: PMC7299283.
41. Ku Z, Xie X, Davidson E, Ye X, Su H, Menachery VD, et al. Molecular determinants and mechanism for antibody cocktail preventing SARS-CoV-2 escape. Nat Commun. 2021;12(1):469. Epub 20210120. doi: 10.1038/s41467-020-20789-7. PubMed PMID: 33473140; PubMed Central PMCID: PMC7817669.
42. Muik A, Wallisch AK, Sänger B, Swanson KA, Mühl J, Chen W, et al. Neutralization of SARS-CoV-2 lineage B.1.1.7 pseudovirus by BNT162b2 vaccine-elicited human sera. Science. 2021;371(6534):1152-3. Epub 20210129. doi: 10.1126/science.abg6105. PubMed PMID: 33514629; PubMed Central PMCID: PMC7971771.
43. Wang P, Nair MS, Liu L, Iketani S, Luo Y, Guo Y, et al. Antibody resistance of SARS-CoV-2 variants B.1.351 and B.1.1.7. Nature. 2021;593(7857):130-5. Epub 20210308. doi: 10.1038/s41586-021-03398-2. PubMed PMID: 33684923.
44. Wibmer CK, Ayres F, Hermanus T, Madzivhandila M, Kgagudi P, Oosthuysen B, et al. SARS-CoV-2 501Y.V2 escapes neutralization by South African COVID-19 donor plasma. Nat Med. 2021;27(4):622-5. Epub 20210302. doi: 10.1038/s41591-021-01285-x. PubMed PMID: 33654292.
45. Wu K, Werner AP, Moliva JI, Koch M, Choi A, Stewart-Jones GBE, et al. mRNA-1273 vaccine induces neutralizing antibodies against spike mutants from global SARS-CoV-2 variants. bioRxiv. 2021. Epub 20210125. doi: 10.1101/2021.01.25.427948. PubMed PMID: 33501442; PubMed Central PMCID: PMC7836112.
46. Andreano E, Piccini G, Licastro D, Casalino L, Johnson NV, Paciello I, et al. SARS-CoV-2 escape. bioRxiv. 2020. Epub 20201228. doi: 10.1101/2020.12.28.424451. PubMed PMID: 33398278; PubMed Central PMCID: PMC7781313.
47. Xie X, Liu Y, Liu J, Zhang X, Zou J, Fontes-Garfias CR, et al. Neutralization of SARS-CoV-2 spike 69/70 deletion, E484K and N501Y variants by BNT162b2 vaccine-elicited sera. Nat Med. 2021;27(4):620-1. Epub 20210208. doi: 10.1038/s41591-021-01270-4. PubMed PMID: 33558724.
48. Dejnirattisai W, Huo J, Zhou D, Zahradník J, Supasa P, Liu C, et al. SARS-CoV-2 Omicron-B.1.1.529 leads to widespread escape from neutralizing antibody responses. Cell. 2022. Epub 20220104. doi: 10.1016/j.cell.2021.12.046. PubMed PMID: 35081335; PubMed Central PMCID: PMC8723827.
49. Kim S, Nguyen TT, Taitt AS, Jhun H, Park HY, Kim SH, et al. SARS-CoV-2 Omicron Mutation Is Faster than the Chase: Multiple Mutations on Spike/ACE2 Interaction Residues. Immune Netw. 2021;21(6):e38. Epub 20211223. doi: 10.4110/in.2021.21.e38. PubMed PMID: 35036025; PubMed Central PMCID: PMC8733186.

50. Dong J, Zost SJ, Greaney AJ, Starr TN, Dingens AS, Chen EC, et al. Genetic and structural basis for SARS-CoV-2 variant neutralization by a two-antibody cocktail. Nat Microbiol. 2021;6(10):1233-44. Epub 20210921. doi: 10.1038/s41564-021-00972-2. PubMed PMID: 34548634; PubMed Central PMCID: PMC8543371.
51. Jaimes JA, André NM, Chappie JS, Millet JK, Whittaker GR. Phylogenetic Analysis and Structural Modeling of SARS-CoV-2 Spike Protein Reveals an Evolutionary Distinct and Proteolytically Sensitive Activation Loop. J Mol Biol. 2020;432(10):3309-25. Epub 20200419. doi: 10.1016/j.jmb.2020.04.009. PubMed PMID: 32320687; PubMed Central PMCID: PMC7166309.
52. Rohaim MA, El Naggar RF, Clayton E, Munir M. Structural and functional insights into non-structural proteins of coronaviruses. Microb Pathog. 2021;150:104641. Epub 20201123. doi: 10.1016/j.micpath.2020.104641. PubMed PMID: 33242646; PubMed Central PMCID: PMC7682334.
53. Fehr AR, Perlman S. Coronaviruses: an overview of their replication and pathogenesis. Methods Mol Biol. 2015;1282:1-23. doi: 10.1007/978-1-4939-2438-7_1. PubMed PMID: 25720466; PubMed Central PMCID: PMC4369385.
54. Chen Y, Liu Q, Guo D. Emerging coronaviruses: Genome structure, replication, and pathogenesis. J Med Virol. 2020;92(10):2249. Epub 20200802. doi: 10.1002/jmv.26234. PubMed PMID: 32881013; PubMed Central PMCID: PMC7435528.
55. Prentice E, Jerome WG, Yoshimori T, Mizushima N, Denison MR. Coronavirus replication complex formation utilizes components of cellular autophagy. J Biol Chem. 2004;279(11):10136-41. Epub 20031229. doi: 10.1074/jbc.M306124200. PubMed PMID: 14699140; PubMed Central PMCID: PMC7957857.
56. Prentice E, McAuliffe J, Lu X, Subbarao K, Denison MR. Identification and characterization of severe acute respiratory syndrome coronavirus replicase proteins. J Virol. 2004;78(18):9977-86. doi: 10.1128/JVI.78.18.9977-9986.2004. PubMed PMID: 15331731; PubMed Central PMCID: PMC514967.
57. Subissi L, Imbert I, Ferron F, Collet A, Coutard B, Decroly E, et al. SARS-CoV ORF1b-encoded nonstructural proteins 12-16: replicative enzymes as antiviral targets. Antiviral Res. 2014;101:122-30. Epub 20131120. doi: 10.1016/j.antiviral.2013.11.006. PubMed PMID: 24269475; PubMed Central PMCID: PMC7113864.
58. Kuijpers TW, Bende RJ, Baars PA, Grummels A, Derks IA, Dolman KM, et al. CD20 deficiency in humans results in impaired T cell-independent antibody responses. J Clin Invest. 2010;120(1):214-22. Epub 20091221. doi: 10.1172/JCI40231. PubMed PMID: 20038800; PubMed Central PMCID: PMC2798692.
59. Casan JML, Wong J, Northcott MJ, Opat S. Anti-CD20 monoclonal antibodies: reviewing a revolution. Hum Vaccin Immunother. 2018;14(12):2820-41. Epub 20180906. doi: 10.1080/21645515.2018.1508624. PubMed PMID: 30096012; PubMed Central PMCID: PMC6343614.
60. Pavlasova G, Mraz M. The regulation and function of CD20: an "enigma" of B-cell biology and targeted therapy. Haematologica. 2020;105(6):1494-506. doi: 10.3324/haematol.2019.243543. PubMed PMID: 32482755; PubMed Central PMCID: PMC7271567.
61. Csizmar CM, Ansell SM. Engaging the Innate and Adaptive Antitumor Immune Response in Lymphoma. Int J Mol Sci. 2021;22(7). Epub 20210324. doi: 10.3390/ijms22073302. PubMed PMID: 33804869; PubMed Central PMCID: PMC8038124.
62. Griggio V, Perutelli F, Salvetti C, Boccellato E, Boccadoro M, Vitale C, et al. Immune Dysfunctions and Immune-Based Therapeutic Interventions in Chronic Lymphocytic Leukemia. Front Immunol. 2020;11:594556. Epub 20201118. doi: 10.3389/fimmu.2020.594556. PubMed PMID: 33312177; PubMed Central PMCID: PMC7708380.
63. Kemp SA, Collier DA, Datir RP, Ferreira IATM, Gayed S, Jahun A, et al. SARS-CoV-2 evolution during treatment of chronic infection. Nature. 2021;592(7853):277-82. Epub 20210205. doi: 10.1038/s41586-021-03291-y. PubMed PMID: 33545711; PubMed Central PMCID: PMC7610568.

64. Weigang S, Fuchs J, Zimmer G, Schnepf D, Kern L, Beer J, et al. Within-host evolution of SARS-CoV-2 in an immunosuppressed COVID-19 patient as a source of immune escape variants. Nat Commun. 2021;12(1):6405. Epub 20211104. doi: 10.1038/s41467-021-26602-3. PubMed PMID: 34737266; PubMed Central PMCID: PMC8568958.
65. Chen L, Zody MC, Di Germanio C, Martinelli R, Mediavilla JR, Cunningham MH, et al. Emergence of Multiple SARS-CoV-2 Antibody Escape Variants in an Immunocompromised Host Undergoing Convalescent Plasma Treatment. mSphere. 2021;6(4):e0048021. Epub 20210825. doi: 10.1128/mSphere.00480-21. PubMed PMID: 34431691; PubMed Central PMCID: PMC8386433.
66. Borges V, Isidro J, Cunha M, Cochicho D, Martins L, Banha L, et al. Long-Term Evolution of SARS-CoV-2 in an Immunocompromised Patient with Non-Hodgkin Lymphoma. mSphere. 2021;6(4):e0024421. Epub 20210728. doi: 10.1128/mSphere.00244-21. PubMed PMID: 34319130; PubMed Central PMCID: PMC8386466.
67. Avanzato VA, Matson MJ, Seifert SN, Pryce R, Williamson BN, Anzick SL, et al. Case Study: Prolonged Infectious SARS-CoV-2 Shedding from an Asymptomatic Immunocompromised Individual with Cancer. Cell. 2020;183(7):1901-12.e9. Epub 20201104. doi: 10.1016/j.cell.2020.10.049. PubMed PMID: 33248470; PubMed Central PMCID: PMC7640888.
68. Jensen B, Luebke N, Feldt T, Keitel V, Brandenburger T, Kindgen-Milles D, et al. Emergence of the E484K mutation in SARS-COV-2-infected immunocompromised patients treated with bamlanivimab in Germany. Lancet Reg Health Eur. 2021;8:100164. Epub 20210714. doi: 10.1016/j.lanepe.2021.100164. PubMed PMID: 34278371; PubMed Central PMCID: PMC8278033.
69. Clark SA, Clark LE, Pan J, Coscia A, McKay LGA, Shankar S, et al. SARS-CoV-2 evolution in an immunocompromised host reveals shared neutralization escape mechanisms. Cell. 2021;184(10):2605-17.e18. Epub 20210316. doi: 10.1016/j.cell.2021.03.027. PubMed PMID: 33831372; PubMed Central PMCID: PMC7962548.
70. Salinas NR, Little DP. 2matrix: A utility for indel coding and phylogenetic matrix concatenation(1.). Appl Plant Sci. 2014;2(1). Epub 20140107. doi: 10.3732/apps.1300083. PubMed PMID: 25202595; PubMed Central PMCID: PMC4123383.
71. Kalyaanamoorthy S, Minh BQ, Wong TKF, von Haeseler A, Jermiin LS. ModelFinder: fast model selection for accurate phylogenetic estimates. Nat Methods. 2017;14(6):587-9. Epub 20170508. doi: 10.1038/nmeth.4285. PubMed PMID: 28481363; PubMed Central PMCID: PMC5453245.

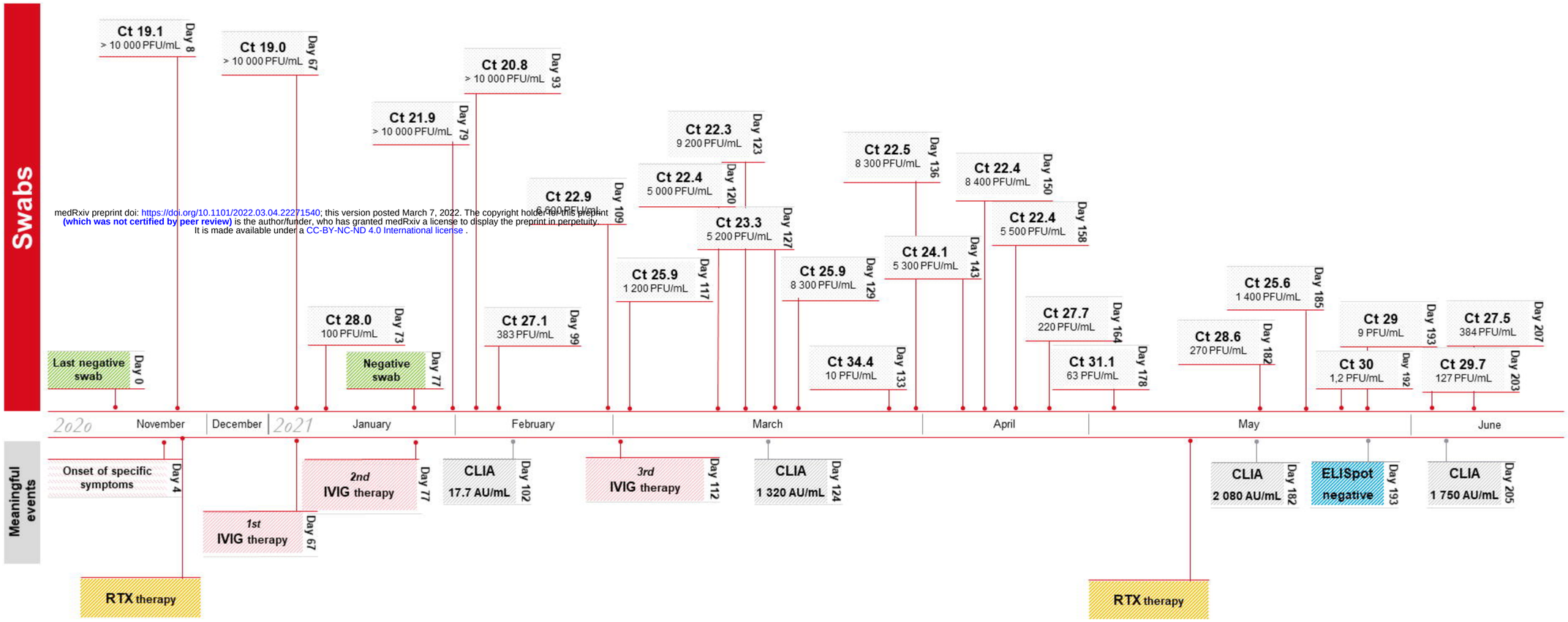

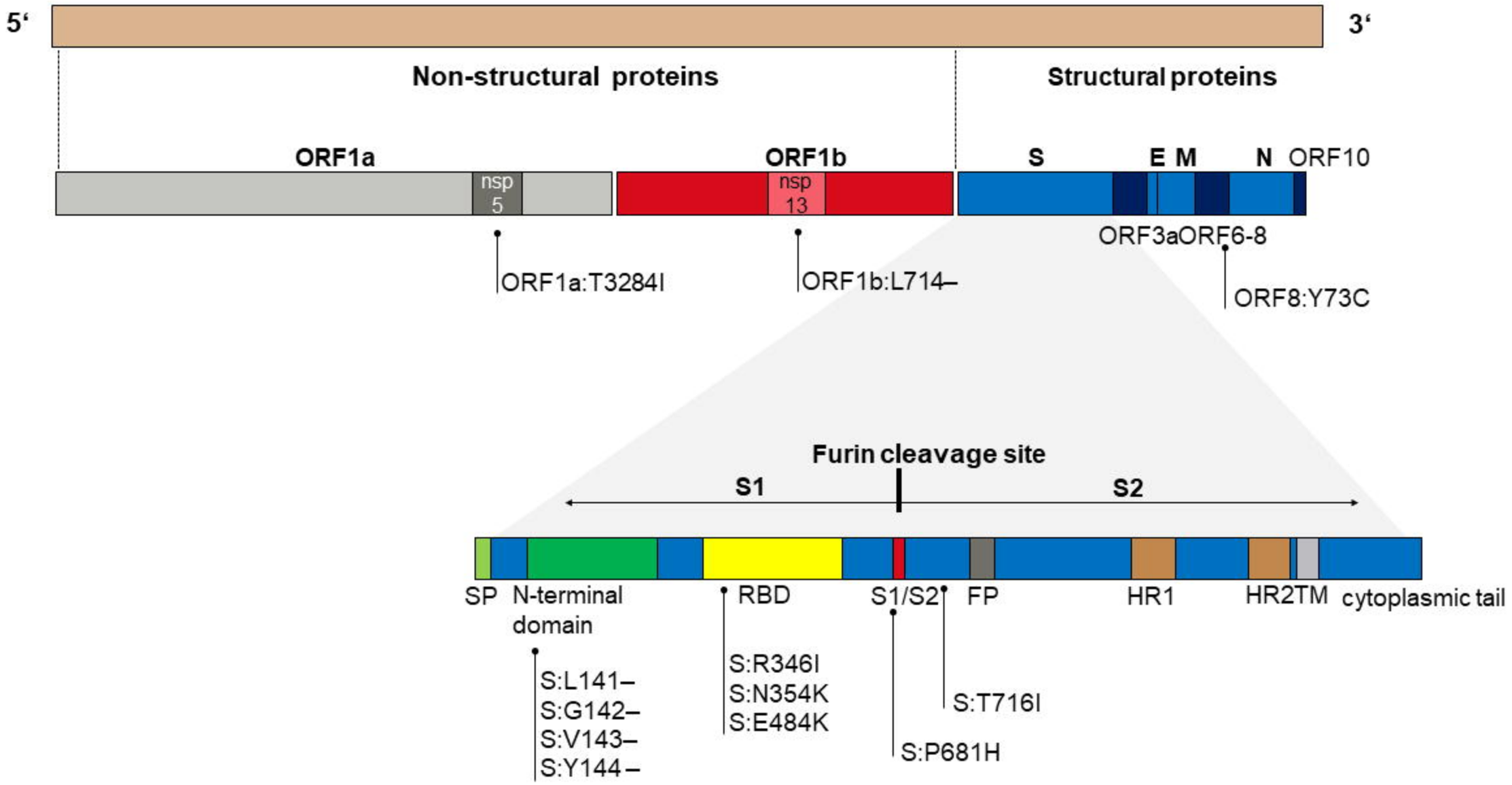
5‘
3‘
Non-structural proteins
Structural proteins
ORF1a
ORF1b
S
E
M
N
ORF10
nsp 5
nsp 13
ORF3a
ORF6-8
ORF1a:T3284I
ORF1b:L714–
ORF8:Y73C
Furin cleavage site
S1
S2
SP
N-terminal domain
RBD
S1/S2
FP
HR1
HR2TM
cytoplasmic tail
S:L141–
S:G142–
S:V143–
S:Y144–
S:R346I
S:N354K
S:E484K
S:P681H
S:T716I

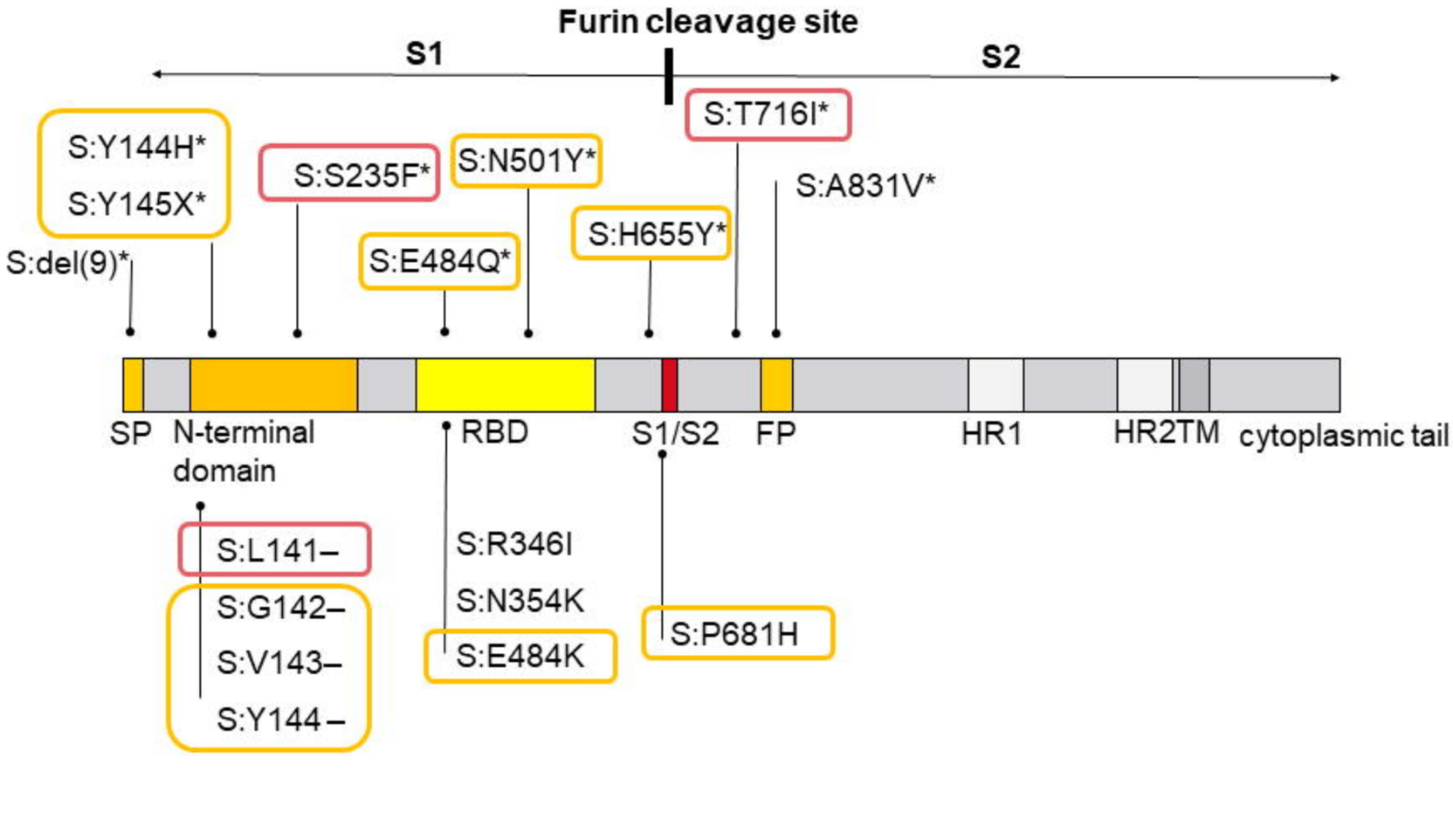
Furin cleavage site
S1
S2
S:T716I*
S:Y144H*
S:Y145X*
S:S235F*
S:N501Y*
S:A831V*
S:H655Y*
S:del(9)*
S:E484Q*
SP
N-terminal domain
RBD
S1/S2
FP
HR1
HR2TM
cytoplasmic tail
S:L141–
S:R346I
S:N354K
S:G142–
S:V143–
S:Y144–
S:E484K
S:P681H

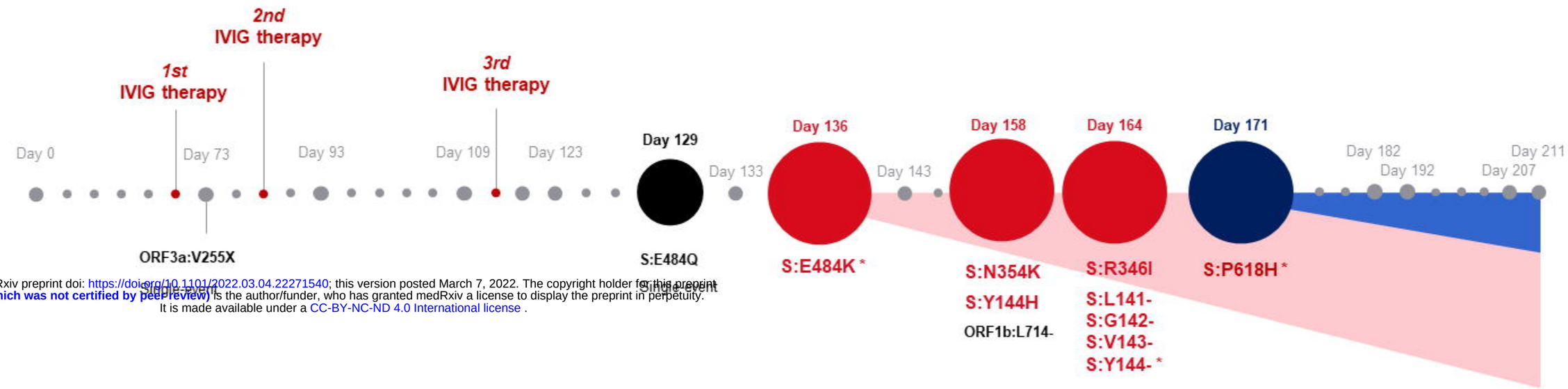

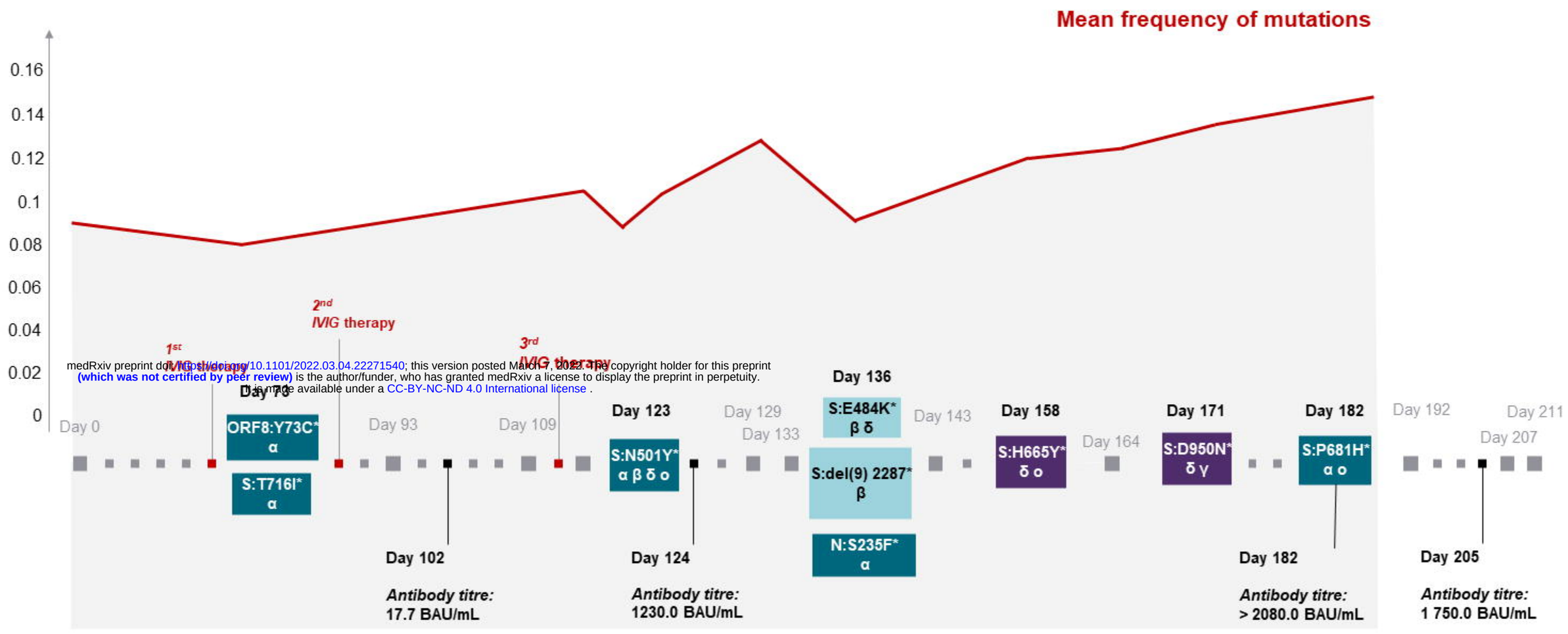

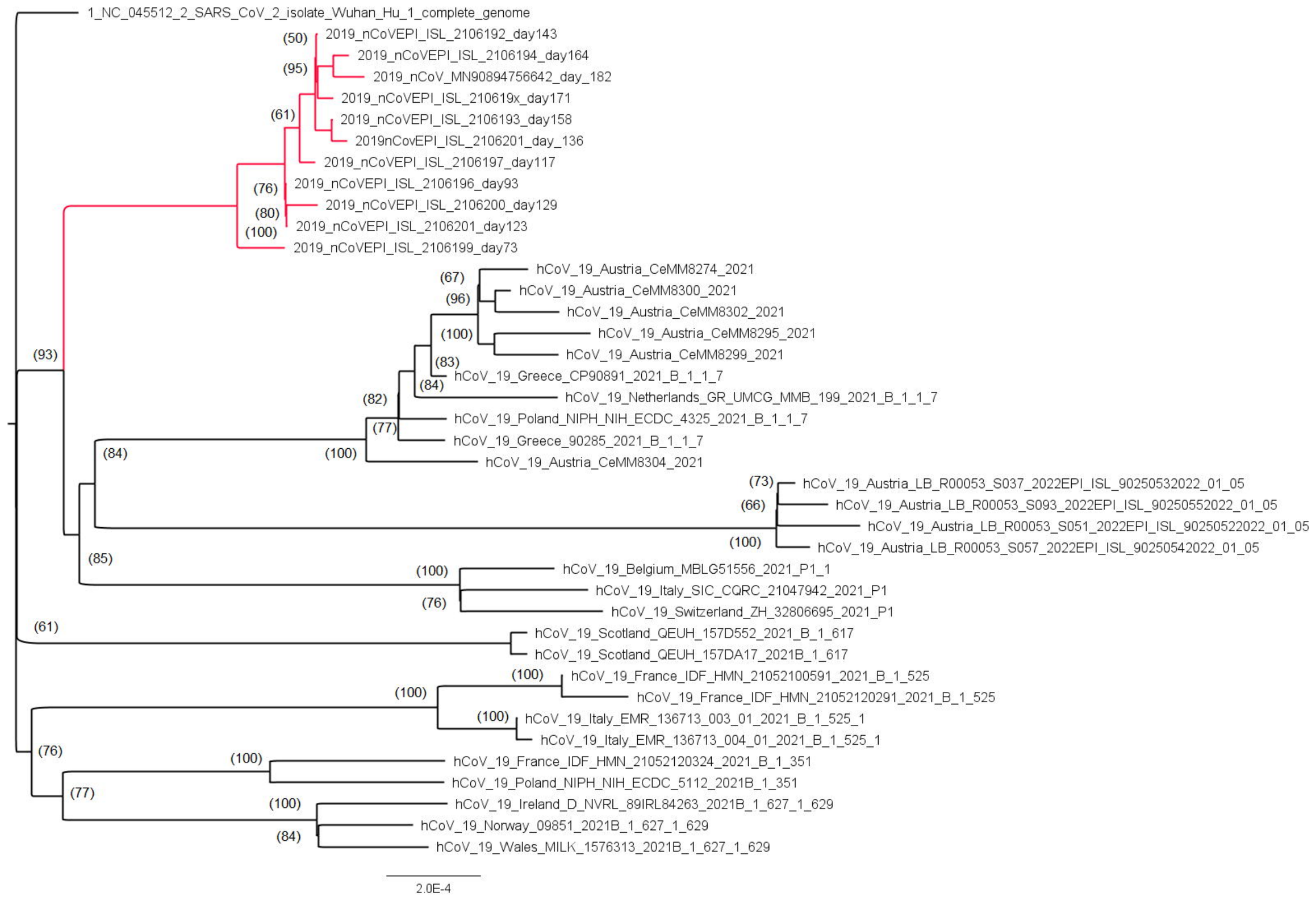
1_NC_045512_2_SARS_CoV_2_isolate_Wuhan_Hu_1_complete_genome
(50)
2019_nCoVEPI_ISL_2106192_day143
2019_nCoVEPI_ISL_2106194_day164
(95)
2019_nCoV_MN90894756642_day_182
2019_nCoVEPI_ISL_210619x_day171
(61)
2019_nCoVEPI_ISL_2106193_day158
2019nCovEPI_ISL_2106201_day_136
2019_nCoVEPI_ISL_2106197_day117
(76)
2019_nCoVEPI_ISL_2106196_day93
(80)
2019_nCoVEPI_ISL_2106200_day129
(100)
2019_nCoVEPI_ISL_2106201_day123
2019_nCoVEPI_ISL_2106199_day73
(67)
hCoV_19_Austria_CeMM8274_2021
(96)
hCoV_19_Austria_CeMM8300_2021
hCoV_19_Austria_CeMM8302_2021
(100)
hCoV_19_Austria_CeMM8295_2021
(93)
hCoV_19_Austria_CeMM8299_2021
(83)
hCoV_19_Greece_CP90891_2021_B_1_1_7
(84)
(82)
hCoV_19_Netherlands_GR_UMCG_MMB_199_2021_B_1_1_7
hCoV_19_Poland_NIPH_NIH_ECDC_4325_2021_B_1_1_7
(77)
hCoV_19_Greece_90285_2021_B_1_1_7
(84)
(100)
hCoV_19_Austria_CeMM8304_2021
(73)
hCoV_19_Austria_LB_R00053_S037_2022EPI_ISL_90250532022_01_05
(66)
hCoV_19_Austria_LB_R00053_S093_2022EPI_ISL_90250552022_01_05
hCoV_19_Austria_LB_R00053_S051_2022EPI_ISL_90250522022_01_05
(100)
hCoV_19_Austria_LB_R00053_S057_2022EPI_ISL_90250542022_01_05
(85)
(100)
hCoV_19_Belgium_MBLG51556_2021_P1_1
hCoV_19_Italy_SIC_CQRC_21047942_2021_P1
(76)
hCoV_19_Switzerland_ZH_32806695_2021_P1
(61)
hCoV_19_Scotland_QEUH_157D552_2021_B_1_617
hCoV_19_Scotland_QEUH_157DA17_2021B_1_617
(100)
hCoV_19_France_IDF_HMN_21052100591_2021_B_1_525
(100)
hCoV_19_France_IDF_HMN_21052120291_2021_B_1_525
(100)
hCoV_19_Italy_EMR_136713_003_01_2021_B_1_525_1
hCoV_19_Italy_EMR_136713_004_01_2021_B_1_525_1
(76)
(100)
hCoV_19_France_IDF_HMN_21052120324_2021_B_1_351
hCoV_19_Poland_NIPH_NIH_ECDC_5112_2021B_1_351
(77)
(100)
hCoV_19_Ireland_D_NVRL_89IRL84263_2021B_1_627_1_629
hCoV_19_Norway_09851_2021B_1_627_1_629
(84)
hCoV_19_Wales_MILK_1576313_2021B_1_627_1_629
2.0E-4